

Investigation of Quantum Phase Transitions using Multi-target DMRG Methods

C. Degli Esposti Boschi¹ and F. Ortolani²

¹ Unità di ricerca INFN di Bologna, e-mail: desposti@bo.infm.it,
viale Berti-Pichat, 6/2, 40127, Bologna, Italia

² Dipartimento di Fisica, Università di Bologna, INFN and INFN, e-mail: ortolani@bo.infn.it,
via Irnerio, 46, 40126, Bologna, Italia

the date of receipt and acceptance should be inserted later

Abstract. In this paper we examine how the predictions of conformal invariance can be widely exploited to overcome the difficulties of the density-matrix renormalization group near quantum critical points. The main idea is to match the set of low-lying energy levels of the lattice Hamiltonian, as a function of the system's size, with the spectrum expected for a given conformal field theory in two dimensions. As in previous studies this procedure requires an accurate targeting of various excited states. Here we discuss how this can be achieved within the DMRG algorithm by means of the recently proposed Thick-restart Lanczos method. As a nontrivial benchmark we use an anisotropic spin-1 Hamiltonian with special attention to the transitions from the Haldane phase. Nonetheless, we think that this procedure could be generally valid in the study of quantum critical phenomena.

PACS. 75.40.Mg Numerical simulation studies – 05.10.Cc Renormalization group methods – 75.10.Pq Spin chain models

1 Outline and General Facts

The density-matrix renormalization group (DMRG) was invented by S. R. White in the early 90's and nowadays is recognized as one of the most accurate and efficient numerical techniques in the study of correlated quantum systems [1]. A number of authors is still contributing to its development for new applications and one of the major points is the dimensionality of the system. While for 1D lattices of spins or electrons there exist several firm results, a generally accepted DMRG scheme in 2D is still lacking despite numerous proposals. However, even for 1D systems, it is known that the DMRG encounters some difficulties in reproducing the physics of quantum critical points. This is because one wants, at the same time, to explore larger and larger system sizes and to maintain a good numerical precision in order to locate the points where the excitation gap closes and to compute the associated critical exponents. If the quantum chain has q states per site, the dimension of the full Hilbert space for L sites grows exponentially as q^L . The main approximation of the DMRG is the truncation to the space spanned by the M eigenvectors of the block density matrix, ρ_b , corresponding to the M largest eigenvalues. The problem is that, close to criticality, the system experiences fluctuations on very large scales and (as will be discussed in sec. 4) the spectrum of ρ_b decays more slowly than in noncriti-

cal cases. Hence if one considers, as a first indicator of the accuracy of the method, the sum of the discarded weights $W_M = \sum_{j>M} w_j$, then this different decay implies that the minimal M to reach a prescribed threshold is generally larger when the system is close to a critical point. To be more specific, Legeza and co-workers [2,3] found that the error in the ground state (GS) energy due to a finite M , at a fixed L , is simply:

$$\delta E_L^{\text{GS}}(M) = E_L^{\text{GS}}(M) - E_L^{\text{GS}}(\infty) \propto W_M. \quad (1)$$

Now, if we admit that the precision for the first excited state follows a similar trend, then there will be a regime, close to the critical point and/or for large L (see sec. 2), where W_M becomes larger than the excitation gap itself. In addition, figs. 3 and 5 of ref. [2] indicate two other important features (at least for the Ising model in a transverse field). First, at criticality the error in the energy at fixed M increases appreciably with the chain's length, and again we see that fixing M once for all, while taking larger and larger values of L , is not a completely safe procedure. The second, and more important point is that the proportionality in eq. (1) holds only after a few *finite-system* iterations have been performed. Using Legeza's terms, these are necessary to cancel the so-called environment error that dominates at sufficiently small L . The crossover from the environment-dominated regime to the truncation-dominated one is marked by a characteristic

size, $L^*(M)$, which increases with increasing M . In sec. 5 we will argue that a similar characteristic length emerges in critical spin-1 chains too. Moreover, in our opinion, the results of Andersson, Boman & Östlund [4] regarding a critical chain of free spinless fermions, or equivalently a spin-1/2 XX model, point somehow in the same direction. Even if the system is known to be rigorously critical, the effect of a finite number of DMRG states is to introduce a *fake correlation length*, that grows as $M^{1.3}$. The interplay between an analogous DMRG length and the true correlation length near the critical temperature of classical 2D systems is also discussed in [5].

We believe that the considerations above indicate that the critical behavior of (1D) quantum systems cannot be “simply” approached by using the computational resources to reach larger and larger values of L by means of the infinite-system DMRG, as it is sometimes done (see, for instance, [6] and refs. therein). Rather, we prefer to exploit as much as possible the consequences of *conformal invariance*. In many cases, indeed, we expect that the low-energy physics of a 1D quantum system near its critical points is described by a suitable conformal field theory (CFT) in (1+1) dimensions [7,8,9,10]. Then, if the system under study has to be critical, we imagine that there will be a scale-invariant effective continuum model that captures its universal features. In 2D the key point is that all these universality classes are encompassed in the framework of CFT. In the last twenty years the numerous exact results in this area have been organized into an elegant framework, which is however too vast for our purposes. Therefore, in sec. 2 we sketch only the points of contact with our analysis and refer to [11] for a comprehensive guide and to [12] for a shorter review on finite-size effects.

However, for a correct interpretation of the DMRG data, and a comparison with a suitable CFT, an accurate calculation of the first excited states at varying L is needed. The targeting of more than one state was proposed by White himself [13] and used by different authors in subsequent papers. A recent comment on this problem can be found in [14]. One of the aims of our work is to test, in connection with the DMRG, the recently proposed Thick-restart Lanczos method [15] to handle a sufficient number of excited states.

2 Identification of the CFT through the Finite-Size Spectrum

The requirement of scale invariance in 2D is sufficiently strong to allow (under general assumptions) a classification of the states of a quantum field theory in terms of the irreducible representations of the Virasoro algebra generated by a set of operators satisfying:

$$[L_m, L_n] = (m-n)L_{m+n} + \frac{c}{12}\delta_{m+n,0}(m^3-m), \quad m, n \in \mathbb{Z} \quad (2)$$

(As is customary in CFT, the statements and equations regarding the holomorphic part should always be suitably

repeated for the antiholomorphic part, denoted by overbars). For unitary theories the central charge of the algebra is either $c \geq 1$, or can be chosen as one of the values $c = 1 - 6/p(p+1)$ ($p = 2, 3, \dots$), each one corresponding to a so-called minimal model. In the latter case, once a $c < 1$ is given, one can decompose the Hilbert space into a *finite* number of irreducible representations of (2) labeled by the eigenvalues of the generator L_0 :

$$L_0|\Delta\rangle = \Delta|\Delta\rangle, \quad \Delta = \frac{[(p+1)r - ps]^2 - 1}{4p(p+1)}, \quad (3)$$

with $1 \leq s \leq r \leq p-1 \in \mathbb{Z}$. More specifically, the primary states $|\Delta\rangle$ are annihilated by L_m with positive m and each one of them generates a conformal family that contains all the states obtained through the application of the negative-integer generators $|\Delta\rangle_m^k = (L_{-m})^k|\Delta\rangle$ (the secondary or descendant states). It can be seen, as a consequence of the Virasoro algebra, that these are in turn eigenvectors of L_0 :

$$L_0|\Delta\rangle_m^k = (\Delta + mk)|\Delta\rangle_m^k. \quad (4)$$

In principle, all the correlation functions of the theory can be reduced to correlators of primary operators. Moreover, the operators L_0 and \bar{L}_0 play a special physical role as can be seen by considering a conformal transformation that maps the plane onto an infinite cylinder, whose circumference of length L represents the space axis with periodic boundary conditions (PBC). Then the energy and momentum operators are simply expressed as:

$$H_{\text{CFT}} = \frac{2\pi v}{L} \left[L_0 + \bar{L}_0 - \frac{c}{12} \right], \quad Q = \frac{2\pi}{L} [L_0 - \bar{L}_0]. \quad (5)$$

Actually, the pre-factor v has been inserted “by hand” in view of the identification of the (critical part of the) spectrum of the original quantum Hamiltonian with the values predicted by the CFT construction. More specifically, the ground state is simply identified with $|\text{vac}\rangle$, for which both L_0 and \bar{L}_0 have null eigenvalues. Thus, the finite-size corrections to the vacuum energy are:

$$E_L^{\text{vac}} = -\frac{\pi c v}{6L}, \quad (6)$$

whereas the excited states follow from the construction of eqs. (3) and (4):

$$E_L(\Delta, m, k; \bar{\Delta}, \bar{m}, \bar{k}) - E_L^{\text{GS}} = \frac{2\pi v}{L} [\Delta + \bar{\Delta} + mk + \bar{m}\bar{k}]. \quad (7)$$

It is important to recall that the sum of the eigenvalues of L_0 and \bar{L}_0 , that is the last term in square brackets $d_O \equiv (\Delta + \bar{\Delta} + mk + \bar{m}\bar{k})$, is called the *scaling dimension* because it enters the algebraic decay of the correlation function of the corresponding operator O :

$$\langle O(0,0)O(z,\bar{z}) \rangle \sim z^{-2(\Delta+mk)}\bar{z}^{-2(\bar{\Delta}+\bar{m}\bar{k})}|_{z=\bar{z}=r} = r^{-2d_O}. \quad (8)$$

In the language of renormalization group (RG) theory, the operators are seen to be relevant when $d_O < 2$, irrelevant

when $d_O > 2$ and marginal when the scaling dimension is exactly 2 (in 2D). The exponents, y_i , of the scaling fields near a fixed point of the RG flow are simply given by $y_i = 2 - d_i$.

The edge case $c = 1$ opens the way to unitary CFT with an infinite number of primary operators. It is related to certain topological constructions of a free bosonic field [16], and the operators (or the associated states) can be further classified in terms of an $\hat{U}(1)$ Kac-Moody algebra. Here we won't enter into more details since ref. [17] is specifically devoted to the study of such $c = 1$ CFT starting from the spin-1 Hamiltonian (12), using just the method explained in the present paper. Finally, when $c > 1$ we have a *continuum* of allowed values and the complexity of the problem in its generality simply forbids us to go on with the discussion of classified cases. We refer to the literature on CFT for general discussions (see, for example, [11, 16]). We will content ourselves with the observation that, at least from an operative point of view, in many cases eqs. (5)-(8) should remain valid once the labels $\Delta, \bar{\Delta}$ and the secondary indices are properly interpreted in terms of wider symmetries that have to be investigated case by case.

The first problem is, of course, that one does not know, *a priori*, which is the CFT that has to be invoked. A great step towards the answer to this question is made if one knows the central charge of the theory, c , that characterizes the underlying Virasoro algebra. Apart from eq. (2) and the operator product expansion of the stress-energy tensor, the central charge appears explicitly in the size-dependence of the GS energy density:

$$\frac{E_L^{\text{GS}}}{L} = e_\infty - \frac{\pi c v}{6L^2}, \quad (9)$$

which is nothing but eq. (6) plus an infinite-size term, which is absent in the formal CFT but has a definite value for a given quantum Hamiltonian. If the quantum chain has open boundary conditions, which are generally better for DMRG convergence, eq. (9) should be modified in two ways [18, 19]. The denominator becomes $24L^2$ and a boundary term B/L should be added, with a non-universal pre-factor B . This term introduces a slower convergence of the GS to the thermodynamic limit (TL) and, at least in this sense, PBC may be more useful for finite-size scaling (FSS) [20].

In quantum field theory the second term of (9) accounts for the Casimir effect [18], while in statistical systems it gives the correction to the free energy at small temperatures (L playing the role of $1/T$ [21]). In our case, eq. (9) is the starting point to discover the CFT that is appropriate for the problem under consideration. Indeed, having good estimates of E_L^{GS} at various L , we can first best-fit e_∞ and cv . Then, if we have reasons to believe that one of the states has scaling dimension 1 (eqs. (7) and (8)), then we can calculate:

$$v = \frac{\Delta E_L(d=1)}{2\pi/L}. \quad (10)$$

If we now interpret $\Delta k = 2\pi/L$ as the quantum of momentum for a chain of length L , then eq. (10) looks like a discrete derivative of the energy vs momentum relation, that is, a group velocity. This somehow explains the term “spin velocity”, which is widely used in the literature of quantum spin chains independently of the real nature of the excitations. Again, the exact form of eq. (10) may vary depending on the boundary conditions. In spin chains with twisted boundary conditions the general relation in eq. (7) remains valid and it's the scaling dimensions of the operators that turn out to depend on the twisting angle [22]. With open boundary conditions, according to ref. [18] the essential modification is the replacement of L by $2L$. This justifies the coefficient of L^2 in eq. (9) and eq. (58) of [19], that looks like eq. (10) with a quantum of momentum $\Delta k = \pi/L$.

Summing up, with a combined usage of eqs. (9) and (10) we can calculate c from the numerical data of the first excited levels for different chain's lengths. Then the identification may fall into two cases. For $c < 1$, unitarity demands that the values of the central charge are quantized, according to the list of minimal models. In this case, a small discrepancy from one of these values is likely to be related to numerical uncertainties. The matter becomes more complicated when one finds a numerical c larger than one, in which case unitarity by itself is not enough to provide a quantization condition. The symmetries of the lattice Hamiltonian in this case are of great help because we expect them to be present also in the corresponding continuum model. Then one may focus on the known 2D field theories whose actions are invariant under both this symmetry group and under conformal transformations. Beside that, when one studies a novel and computationally demanding system it may be very useful to get a first insight of the CFT by performing a finite-size analysis of DMRG data obtained with the infinite-system algorithm and open boundary conditions, as in [19]. Nonetheless, we discourage a blind usage of the infinite-system DMRG to conclude (as in ref. [6]) that the numerical discrepancies from the expected values are to be ascribed to nontrivial effects beyond the CFT framework. If in doubt, the final answer should always come from a careful refinement using *finite-system* numerical data, in a range of L where the scaling behavior is visible but the accuracy is not corrupted significantly by the DMRG truncation error.

In any case, what we are actually performing is a self-consistent guess of the underlying CFT. In principle, this allows an analytical calculation of the scaling dimensions, d_ℓ , of all the operators associated with the excited states. The corresponding energy gaps, here formally indexed by ℓ , scale according to eq. (7):

$$\Delta E_L^\ell = \frac{2\pi}{L} v d_\ell. \quad (11)$$

Matching the numerical spectrum of a certain number of levels with the structure encoded in the scaling dimensions of eq. (11) represents a particularly stringent test of the hypothesis made.

3 Model and Details of the Implementation: Multi-target Method

Following our previous paper [17] we have considered the following spin-1 Hamiltonian:

$$H = \sum_j \left[\frac{1}{2} (S_j^+ S_{j+1}^- + S_j^- S_{j+1}^+) + \lambda S_j^z S_{j+1}^z + D (S_j^z)^2 \right] \quad (12)$$

for a chain of L spins which includes both an Ising-like and a single-ion anisotropy term, with coefficients λ and D respectively. Formally we have set $\hbar = 1$ and the overall coupling constant $J = 1$ so that every quantity turns out to be dimensionless and we have imposed PBC: $\mathbf{S}_{j+L} = \mathbf{S}_j \quad \forall j = 1, \dots, L$. See [17, 23, 24, 25, 26, 27] for a discussion of the various phases in the λ - D diagram.

The algorithm that we have implemented for DMRG calculations follows rather closely the lines indicated by White in his seminal papers [13, 28]. As regards our specific application, we should outline the following points.

The superblock geometry was chosen to be $[\mathbf{B}^r \bullet | \mathbf{B}_{\text{ref}}'^\bullet]$ with PBC, where $\mathbf{B}_{\text{ref}}'^\bullet$ is the (left \leftrightarrow right) reflection of block $\mathbf{B}^{r'}$ with r' sites. The rationale for adopting this configuration is that, being effectively on a ring, the two blocks are always separated by a single site, for which the operators are small matrices that are treated exactly (no truncation) [13]. In this way we expect a better precision in the correlation functions calculated by fixing one of the two points on these sites and moving the other one along the block. In a recent application of the DMRG to quantum chemistry calculations [3] it has been pointed out that the configuration of the superblock may be one of the major points of optimization of the method for future applications. As regards the choice of the boundary conditions, we are aware of the fact that with open conditions a smaller M is generally required and that in certain cases (i.e. Gaussian transitions) the introduction of twisted boundary conditions is a clever trick to identify the critical point using numerical data on relatively small systems [22, 27, 29, 30]. Nevertheless, in our set of calculations we have adopted PBC to get rid of the edge effects that in some cases mask almost all the information contained in very short-ranged (string) correlation functions. Moreover, we are primarily interested in the transitions from the Haldane phase, for which it is known that the finite-size GS acquires a fourfold degeneracy due to the two free effective spins at the ends of the chain [26]. With PBC instead, one has a unique finite-size GS so that the convergence of the Lanczos procedure is better and the analysis of the numerical gaps is simpler.

We used the finite-system algorithm with three iterations. This prescription should ensure the virtual elimination of the so-called environment error [2], which is expected to dominate in the very first iterations for $L < L^*(M)$ (see below). In fact, it is only after a suitable number of such sweeps that we may expect that the error in the energies has been minimized (for a given L and M) and eq. (1) holds true. Normally the correlations are computed at

the end of the third iteration, once the best approximation of the GS is available.

Dealing with quantum spin chains, we always exploit the conservation of the z -component of the total spin, M^z . Typically we are interested in nonmagnetic GS's, that is, with $M^z = 0$. In every studied case the correlations have been calculated targeting only the lowest-energy state within this sector. However, in order to analyze the energy spectrum, we had to target the lowest-energy state(s) in the other sectors $|M^z| = 1, 2, \dots$ and/or target also a few excited states within the $M^z = 0$ sector, depending on the phase under study. The standard Lanczos algorithm gives with enough precision the ground state of the system, but it is not so accurate for the excited states. Moreover, as a consequence of a general theorem on tridiagonal symmetric matrices, we can't have degenerate states from this method. So the algorithm must be modified to allow the building of the reduced density matrix over the block as a mixture of the matrices corresponding to each target state. While for the latter point we are not aware of any specific "recipe" other than that of equal weights, the implementation of the multi-target diagonalization routine within our DMRG code is based on the Thick-restart Lanczos method recently introduced by Wu and Simon [15]. In principle, the strategy used here does not rely on a particular algorithm to extract a group of eigenvalues of the superblock Hamiltonian. The methods commonly used so far are the Davidson-Liu and the block Lanczos. Our choice of the Thick-restart Lanczos was based on the intention of testing and exploiting the stability of the method, as claimed by the authors [15]. Moreover, its implementation is a simple extension of the standard Lanczos procedure, as described in appendix A.

Once M^z is fixed, in a given run we wish to follow simultaneously the first levels $|M^z; \mathbf{b}\rangle$ with $\mathbf{b}=0, 1, 2, \dots, \mathbf{t}$ (the GS being identified by $(M^z = 0; \mathbf{b} = 0)$). Then, as in the conventional Lanczos scheme, we have to iterate until the norms of the residual vectors and/or the differences of the energies in consecutive steps are smaller than prescribed tolerances ($10^{-9} - 10^{-12}$ in our calculations). The delicate point to keep under control is that, once the lowest state $|M^z; 0\rangle$ is found, if we keep iterating searching for higher levels the orthogonality of the basis may be lost, just because the eigenvectors corresponding to these levels tend to overlap again with the vector $|M^z; 0\rangle$. As a result, the procedure is computationally more demanding because one has to re-orthogonalize the basis from time to time. We have seen that this part takes a 10-20% of the total time spent in each call to the Lanczos routine. We have also observed that if this re-orthogonalization is not performed, one of the undesired effects is that the excited doublets (typically due to momentum degeneracy) are not computed correctly. More specifically, it seems that while the two energy values are nearly the same in the asymmetric stages of the sweeps, when the superblock geometry becomes symmetric ($r = r'$ in the notations of the preceding point) the double degeneracy is suddenly lost in a spurious way. This is in line with the results of ref. [3], where the error in the energy is kept under control

by means of a dynamically-adjusted M and the configurations that require a larger number of DMRG states are just those near the symmetric one.

4 Dependence on the Number of DMRG States

As discussed in the introduction of sec. 1 the choice of the number of optimized states with respect to the chain length L is the crucial point to address in any DMRG calculation. Being conscious that the energy accuracy is *not* an exhaustive indicator, from eq. (1) one should try, at least, to keep the discarded weight W_M as small as possible. This quantity, in turn, is related to the decay of the density matrix eigenvalues $\{w_j\}$ as a function of the index j :

$$W_M = \sum_{j>M} w_j = \sum_j D_j z_j, \quad (13)$$

where the last equality is a simple rewriting in terms of the degeneracies D_j and of the distinct eigenvalues z_j . The issue appeared to be important from the very beginning and is the core to the success of the DMRG. In [13,31] it was argued that the convergence of the GS energy of a gapped or a spatially finite system is roughly exponential in M :

$$\delta E_L \propto e^{-M/M^*(L)}, \quad (14)$$

with a superimposed step-like behavior, probably related to the successive inclusion of more and more complete spin sectors. It is also generally believed that this exponential decay becomes slower (possibly algebraic) when a critical point is approached. At this stage it is interesting to recall that for integrable systems the spectrum of ρ_b can be determined exactly. In fact, it is known [5,9] that for a quantum chain the infinite-size block density matrix is given by $\rho_b = \chi^4$, where χ is the corner transfer matrix of the associated 2D classical statistical system. This statement has a wide generality, with the exception of critical cases where the boundary effects may have some role and are expected to affect the tails of the distribution [32]. For integrable systems a further step can be made: χ is expressed as the exponential of a pseudo-Hamiltonian, K , that involves the same local operators of the Hamiltonian (e.g. $S_j^\alpha S_{j+1}^\alpha$) but with coefficients depending on the site index j . Moreover, the spectrum of K can be determined exactly and, typically, the eigenvalues turn out to be equally spaced. Therefore the distinct eigenvalues of ρ_b decay as:

$$z_j \propto Z^j, \quad Z = e^{-\epsilon}, \quad (15)$$

$\epsilon/4$ being the level spacing of $-K$. These predictions have been explicitly verified for the Ising model in a transverse field [9] and for the XXZ spin-1/2 Heisenberg chain [9,10].

Now we shall try to elucidate this topic in the case of critical spin-1 systems using the Hamiltonian of eq. (12). At $(\lambda = 1, D = 0)$ one has an isotropic anti-ferromagnetic (AF) Heisenberg chain of integer spin, whose theoretical interest comes from what is now known as Haldane's

conjecture [33], that predicts a genuine quantum behavior with a finite energy gap in the excitation spectrum. This has to be contrasted with what happens in half-odd-integer cases that are gapless (i.e. critical) in the thermodynamic limit. Another important theoretical contribution is the mapping between spin chains and restricted solid-on-solid models proposed by den Nijs and Rommelse [34]. Qualitatively, the Haldane phase is interpreted as a spin-liquid, in the sense that the effective particles - the spin state $|0\rangle$ represent an empty site and $|\pm\rangle$ represent a particle with spin up or down - are positionally disordered but carry anti-ferromagnetic order. In the quantum states that contribute to the GS, this order is hidden by arbitrarily long strings of $|0\rangle$'s but can be measured by the string order correlators [26,34]:

$$O_S^\alpha(j, k) \equiv - \left\langle S_j^\alpha \exp \left(i\pi \sum_{n=j+1}^{k-1} S_n^\alpha \right) S_k^\alpha \right\rangle, \quad (16)$$

(the expectation value being taken on the GS) and their asymptotic order parameters, $O_S^\alpha \equiv \lim_{|j-k| \rightarrow \infty} O_S^\alpha(j, k)$.

Beside that, nowadays there exist several experimental realizations of these anisotropic spin-1 chains: to the author's knowledge, RbNiCl_3 [23] and Y_2BaNiO_5 [35,36] are examples of pure Haldane systems, CsNiFe_3 is a ferromagnet ($\lambda = -1$) with appreciable single-ion anisotropy ($D \simeq 0.4$) and $\text{CoCl}_2 \cdot 2\text{H}_2\text{O}$ behaves as an Ising ferromagnet ($|\lambda| \gg 1$) with high easy-axis anisotropy ($D \simeq -5$) [24,37]. The so-called NENP [38,39] and NENC [40] represent, respectively, small- D ($\simeq 0.2$) and large- D ($\simeq 7.5$) antiferromagnets with easy-plane anisotropy.

In order to study the convergence of truncation errors close to criticality we have selected a pair of representative points in the phase diagram. In the origin ($\lambda = 0, D = 0$), where a Berezinskii-Kosterlitz-Thouless (BKT) transition is expected [41], we have the spin-1 analogue of the XX spin-1/2 model used in ref. [4] to examine the effect of a finite M on a quantum critical system. The second point that we will examine in this section is $(\lambda = 1, D = 0.95)$ because from refs. [17,30] we know that it lies very close to the line of transition from the Haldane phase to the so-called large- D phase. In the following numerical analysis these two points will be denoted by XX and H-D, respectively. The results can be thought as the critical counterpart of the ones presented in [10] for an isotropic spin-1 Heisenberg chain.

For the H-D point we have computed the first excited state in the sectors with $M^z = 0, 1$ for $L = 16, 20, 24, 32, 48$ and 64, using $M = 81, 162, 243, 324$ and 405 DMRG states for each case. For the XX point, we have monitored the same states for the same values of M using also $L = 28$. The exponential decay of eq. (14) seems to be adequate in all the cases, as shown in fig. 1. For every fixed L we best-fit the energy-vs- M data and read off the characteristic values $M^*(L)$, represented in fig. 2. Of course, the larger L is the larger M^* is, and it seems that the curves do not saturate indicating, as is reasonable, that a finite M is not enough to describe properly a (quasi-)critical system with arbitrarily large L . However, the promising

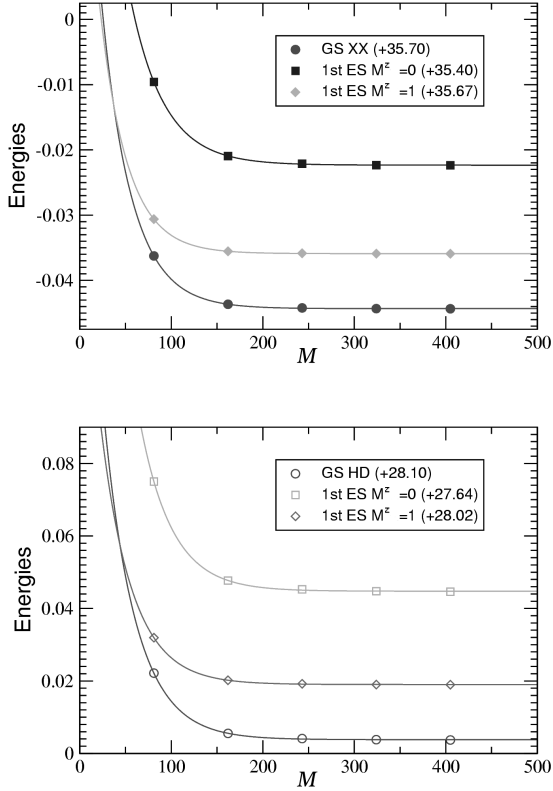


Fig. 1. Energies of the GS and of the first excited states within $M^z = 0, 1$ at the points XX and H-D (see text). The symbols represent DMRG values obtained with $L = 32$ and an increasing number of DMRG states while the continuous lines are exponential fits. For clarity reasons, the offsets reported in the legend have been added.

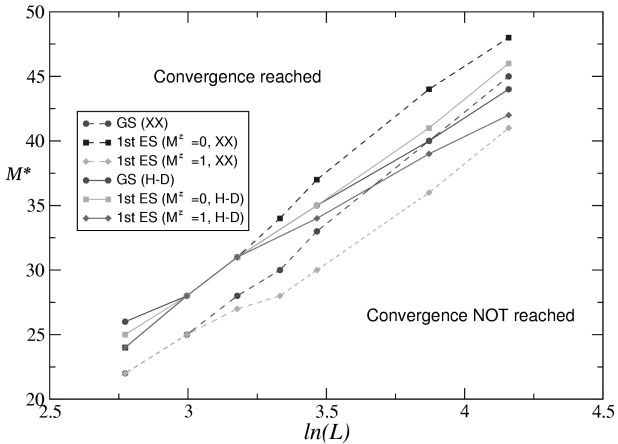


Fig. 2. Exponential factor $M^*(L)$ (eq. (14)) for the points indicated in the legend (see text). The lines separate two regions where the convergence of the low-lying levels with M is essentially reached or not.

Table 1. Slopes M_0 of the best fits of the sets plotted in fig. 2 (with same notations). [†] Only with $L \geq 28$; [‡] Only with $L \geq 24$.

Data Set	M_0
GS XX	16.9 ± 0.4
1st $M^z = 0$	17.6 ± 0.4
1st $M^z = 1$ [†]	15.6 ± 0.4
GS H-D	13.2 ± 0.3
1st $M^z = 0$	15.0 ± 0.2
1st $M^z = 1$ [‡]	11.4 ± 0.3

feature of fig. 2 is that the various data sets approximately lie in a strip of the $M - \ln L$ plot, characterized by a linear slope $M_0 = 15 \pm 3$. More precisely, this value is an overall measure of the slopes of the best-fit straight lines, reported in table 1 for the six sets considered. In other terms, if we invert the relation between M and L , we find $L^*(M) \propto \exp(M/M_0)$, which means that for fixed M we expect a good convergence of the energies for $L < L^*(M)$ (negligible truncation error, in the language of [2]) and that the gain in increasing M is exponential with a surprisingly small reference value M_0 (in line with the first observations of White himself [13]). Interestingly enough, the logarithmic behavior of $M^*(L)$ can be justified by taking eq. (15) to be valid even at critical points. There one expects $\epsilon \rightarrow 0$ and indeed conformal invariance indicates that the finite-size level spacing vanishes as $\epsilon = \epsilon_0 / \ln L$ (with ϵ_0 a constant) [9]. Now, if we approximate the discarded weight of eq. (13) ignoring the degeneracy factor D_j , we readily get:

$$W_M = \sum_{j>M} Z^j = \frac{Z}{1-Z} Z^M \simeq \frac{\ln L}{\epsilon_0} e^{-\epsilon_0 M / \ln L}. \quad (17)$$

Unfortunately, the effective accuracy gets poorer, by one or two orders of magnitude [3], when we deal with correlation functions. Keeping the errors in the low-lying levels below the desired threshold may not be sufficient so that we had to adopt an additional criterion to decide whether the selected M is large enough or not. In practice, we check systematically the properties of translational and reflectional invariance that we expect from the symmetries of the Hamiltonian. In fact we have observed that of one the “symptoms” for a too-small M is the visible (i.e. above numerical uncertainties) lack of some of these invariances. To be more specific, if $C(0, k)$ is a certain correlation function computed starting at $j = 0$, we have always increased M (at the expense of L) until the bound $|C(L/2, L/2 \pm k) - C(0, k)| / |C(0, k)| \lesssim 0.05$ was met for k varying from 0 to $L/2$, possibly with the exception of the ranges where $C(0, k)$ is very small, say 10^{-6} . In fig. 3 we give an example with string correlation functions (eq. (16)) at the XX point. These should be translationally invariant but their numerical estimates depend in fact on the starting point j because we have intentionally fixed a too-small value, $M = 50$. It is also interesting to point out that in this example $O_S^x(j, j+r)$ essentially coincides with

$(-)^r \langle S_j^x S_{j+r}^x \rangle$ (not plotted). We interpret this coincidence with the onset of planar order at the BKT transition. At the XX point both the transverse and the longitudinal string order parameters are expected to vanish (sec. II of [42]), and the fact that the minimum of the x -data in fig. 3 is about ~ 0.3 is to be interpreted as a finite-size effect. In a similar way, a preliminary study of the 1D Hubbard model with bond-charge interaction near its critical points [43] indicates that in order to obtain accurate correlation functions it is necessary to use a large number of DMRG states (> 500) and several finite-system iterations. From the literature it turns out that this is a general feature of electronic systems, like Hubbard models and critical variants.

Finally, we mention the relevance for ref. [44], where the thermal behavior of the quantum 1D and 2D $S = 1$ XX model is studied by means of the two-time Green's function method. The adopted decoupling scheme requires the calculation of the on-site, nearest-neighbor and next-to-nearest-neighbor ordinary correlations in the x and z channel:

$$C_0^{x,z} \equiv \langle (S_0^{x,z})^2 \rangle, \quad C_1^{x,z} \equiv 1/2[\langle S_0^{x,z} S_1^{x,z} \rangle + \langle S_0^{x,z} S_{L-1}^{x,z} \rangle]$$

$$C_2^x \equiv 1/2[\langle S_0^{x,z} S_2^{x,z} \rangle + \langle S_0^{x,z} S_{L-2}^{x,z} \rangle], \quad (18)$$

(as in eqs. (14) and (15) of [44] even if it is not clear if C_2^x should include the on-site term with $\delta = -\delta'$ or not). It is explicitly said that an exact term of comparison in 1D at $T = 0$ would be needed in order to check more precisely their methodology. Though in principle approximate, the DMRG data can be regarded as a solid benchmark. We have computed the five numbers above with $M = 300$ for $L = 32, 48, 64, 80, 100$. Having to do with short-range non-vanishing quantities, the size dependence is very weak (fourth decimal place or better) and an algebraic extrapolation to $L \rightarrow \infty$ yields $C_0^x = 0.7577$, $C_0^z = 0.4846$, $C_1^x = 0.5579$, $C_1^z = -0.1778$ and $C_2^x = 0.464$ (not including the on-site term). From a direct comparison with table I of [44] we see that with their choices of the decoupling parameters the largest discrepancy affects C_2^x with a relative difference of about 20%.

5 Examples and Results

The quality of the numerical analysis of the critical properties depends heavily on the location of the critical points of interest. At present, our study focuses primarily on the transitions from the Haldane phase, for which it is convenient to fix some representative values of λ and let D vary across the phase boundaries. This preliminary task of finding $D_c(\lambda)$ turns out to be crucial for subsequent calculations and is divided into two steps.

First, one gets an approximate idea of the transition points using a direct extrapolation in $1/L$ of the numerical values of the gaps, computed at increasing L with a moderate number of DMRG states. Clearly, one may want to explore a rather large interval of values and so the increments in D will not be particularly small (say 0.1). An

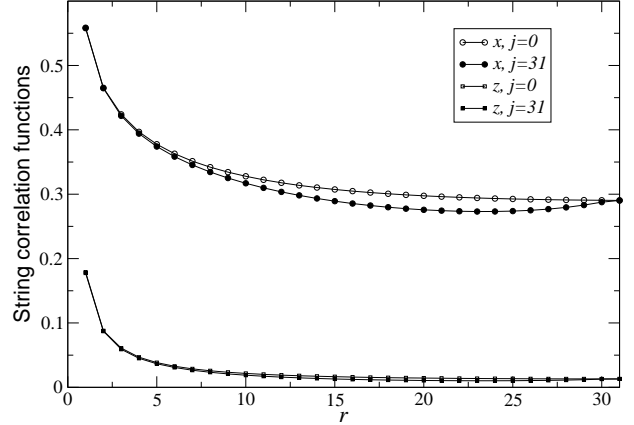


Fig. 3. Transverse ($\alpha = x$, circles) and longitudinal ($\alpha = z$, squares) string correlation functions for a chain of 64 sites with PBC at the XX point (see text), computed with only $M = 50$ DMRG states. The empty symbols represent $O_S^\alpha(j = 0, r)$ while the full ones represent $O_S^\alpha(j = 31, 31+r)$, with an evident dependence on j .

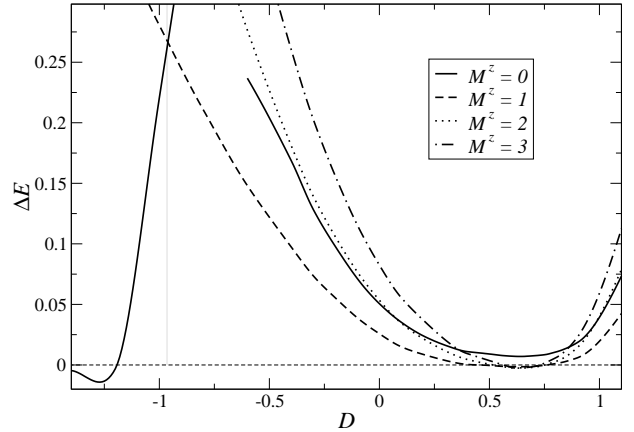


Fig. 4. Extrapolations of the gaps between the GS and the first excited states within the indicated sectors of M^z at $\lambda = 0.5$. The values for $L \rightarrow \infty$ have been obtained through a quadratic best fit in $1/L$ from the data at $L = 32, 48, 64, 80$ with 216 DMRG states. For graphical convenience, the various sets have been turned into continuous curves using splines. The vertical gray line indicates the point of intersection between the states with $M^z = 0$ and $M^z = 1$, that is, the analogue of the Haldane triplet at $\lambda = 0.5$.

example of such a scanning at $\lambda = 0.5$ is presented in fig. 4. Note that at $(\lambda = 0.5, D \simeq 0.6)$ one has a first insight of the “cascade” of levels predicted by CFT (eq. (7) for $L \rightarrow \infty$.)

As a second step, the analysis must be refined around the minima of the curves ΔE -vs- D with smaller increments in D and a larger value of M . According to FSS theory ([45] and appendix B), at the true critical point (that is, in the TL) one should see that the data settle to a constant in the log-log plot of the scaled gaps vs L . Fig. 5 shows an example of such an inspection for $\lambda = 0.5$ and D varying about the H-D transition. It is seen that

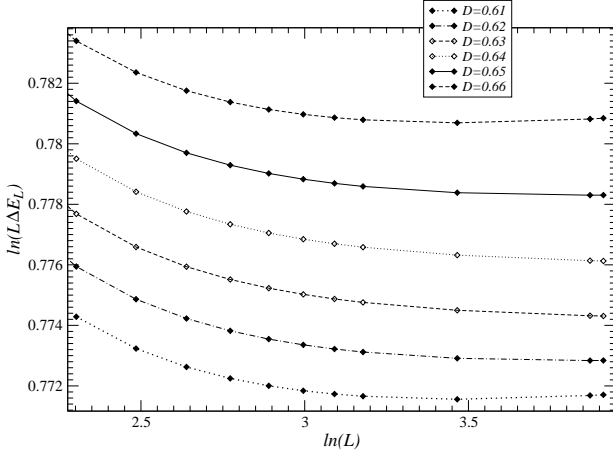


Fig. 5. H-D transition at $\lambda = 0.5$: Scaled gaps (between $|M^z = 0, b = 0\rangle$ and $|M^z = 1, b = 0\rangle$) at $L = 10, 12, 14, 16, 18, 20, 22, 24, 32, 48, 50$ (with 400 DMRG states), for the values of D indicated in the legend.

the differences in the slopes of the various curves are not so pronounced. Hence, from this plot we have selected two candidates for the critical point $D_c(0.5)$, namely $D = 0.62$ and $D = 0.65$. At this stage we should mention that in this type of transition the phenomenological renormalization group (PRG) method [45] also typically yields a pair of (pseudo-)critical values at fixed L . In this case, these two sequences of values seem to converge to the point $D = 0.62$ (but in order to see convergence of the curves up to $L = 50$ we had to use 400 DMRG states). Unfortunately, this turns out to be an invalid tie-break because at this point the finite-size β -function (eq. (37)) increases with increasing L . This is shown in fig. 6, where $\beta_L(0.65)$ is also plotted. The latter scales to zero with a size-dependent slope that we calculate from eq. (38). The extrapolation to $1/L \rightarrow 0$ (and restricted to $L \geq 22$) then gives $\nu = 3.69 \pm 0.04$. As discussed below this is not a particularly good estimate of ν . Nonetheless, the location of the critical point $D_c(0.5) = 0.65$ is quite close to the value $D = 0.635$ obtained in ref. [27] with a method based on twisted boundary conditions and exact diagonalization up to $L = 16$. In this sense, we suspect that the difficulties encountered both with FSS and PRG (roughly speaking, the “splitting” of critical points) are due to the peculiar structure of the energy spectrum in this type of transition. In particular, both sides of the transition are massive and it is likely that with PBC we are faced with the scenario proposed by Kitazawa [22]: In eq. (35) the constant $C^{(1)}$ for the first excited state could vanish and we have to consider a second-order expansion in $(D - D_c)$. Consequently, the values of the critical points are determined via parabolic intersections that are more sensitive to numerical uncertainties. Probably this is also the reason why the scaling analysis of β_L as used here performs poorly. In fact, in our framework the best estimate of ν comes from another method, namely via the scaling dimension of the mass-generating operator. According to the discus-

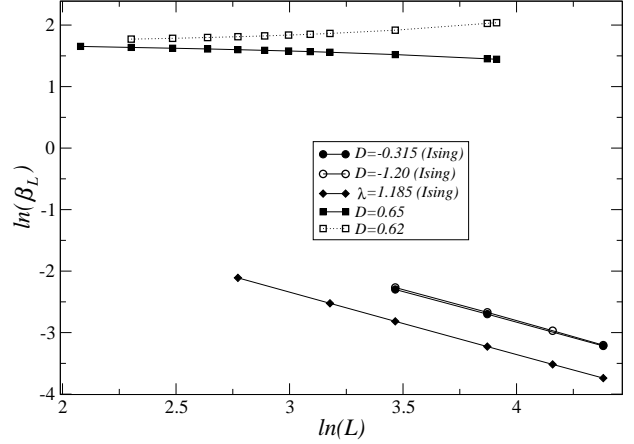


Fig. 6. Finite-size β -functions for $(\lambda = 0.5, D = 0.62)$ (open squares), $(\lambda = 0.5, D = 0.65)$ (full squares), $(\lambda = 0.5, D = -1.2)$ (open circles), $(\lambda = 1, D = -0.315)$ (full circles) and $(\lambda = 1.185, D = 0)$ (full diamonds). All the numerical derivatives have been calculated by means of centered differences with $\delta D = 0.01$ for the first two cases (Haldane-large- D transition), $\delta D = 0.005$ for the second two and $\delta \lambda = 0.005$ for the last one. Notice that the three lines for the transitions from the Haldane to the Néel-like phase (Ising type) have essentially the same slope, that is, the same ν (see also the discussion at the end of sec. 5).

sion that follows, for $(\lambda = 0.5, D = 0.65)$ we find $\nu = 2.38$, essentially in accord with the values given in [24].

At the transition between the Haldane and the Néel-like phase (henceforth denoted as H-N) these difficulties regarding the location of the critical points and the scaling to zero of β_L are not experienced. Let us work out in detail the λ -driven transition at $D = 0$, that has been recently revisited [6] to argue that it does not belong to the Ising universality class, as is generally accepted. Taking advantage of previous results, we fixed $D = 0$ in eq. (12) and varied λ about 1.18. In fig. 7(a) we report the L -dependent pseudo-critical values obtained by solving numerically the PRG equation [45]:

$$\frac{[(L + \delta L)\Delta E_{L+\delta L}(\lambda_{pc}) - L\Delta E_L(\lambda_{pc})]}{\delta L} = 0. \quad (19)$$

Our best-fit critical value in the TL turns out to be $\lambda_c(D = 0) = 1.1856$ (see caption), in agreement both with [29] and with [6]. This point separates a gapfull phase, where the scaled gap increases with increasing L , from a gapless one (doubly degenerate GS), where it is expected that the scaled gap converges rapidly to zero [23]. The algebraic decay of β_L is rather evident from fig. 6 and one can readily estimate $\nu = 0.987 \pm 0.002$ from the slope of the linear best fit. This is the first indication that the H-N transition belongs to the (2D) Ising universality class, as reported by various authors (see below our argument based on the combined use of CFT and DMRG).

Despite some difficulties in locating the critical points of the H-D line on the basis of DMRG data, we are now in position to suggest an extension in the usage of this nu-

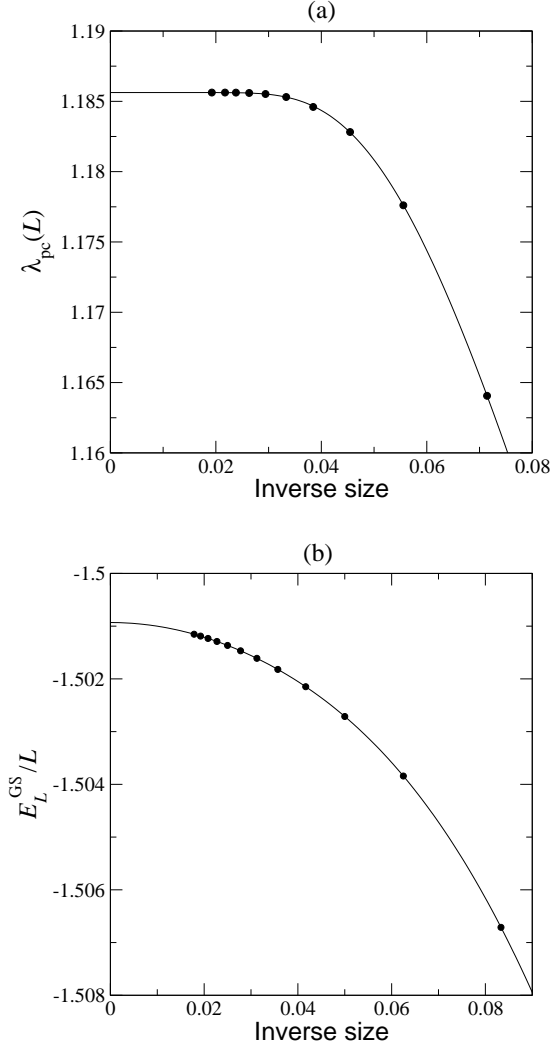


Fig. 7. (a): PRG location of the Ising-like critical point λ_c at $D = 0$. The pseudo-critical values of λ (full circles) are plotted against the inverse of the middle size, $(L + \delta L/2)^{-1}$, and correspond to L ranging from 12 to 48 in steps of $\delta L = 4$ (see eq. (19)) using $M = 405$. The continuous line is a best-fit of the form $\lambda_c - AL \exp(-L/L_{PRG})$ with $A = 0.1185$ and $L_{PRG} = 3.224$. (b): Extrapolation (continuous line) of the GS energy density (full circles) according to the form discussed in the text.

merical method to approach the critical points of quantum Hamiltonians. Taking advantage of the underlying conformal theory that should be present in all these cases, we focus on the finite-size energy spectrum, as summarized by eqs. (7) and (9). Once the critical point is located, we select a number of states that seem to become degenerate with the GS in the limit $L \rightarrow \infty$. Then we consider $L\Delta E_L/2\pi$ and plot the data against $1/L$ to see whether they settle to a constant, which represents the associated scaling dimension d_ℓ multiplied by the velocity v . Actually, due to this pre-factor we have to imagine a self-consistent procedure: Depending on the type of the transition we have in mind (that is, depending on the con-

formal anomaly c), we stick on one or more levels in the spectrum that have exactly $d = 1$. Hence the value for $1/L \rightarrow 0$ is nothing but v . Once the velocity is estimated, one uses eq. (9) to best fit the product cv and see if the value of c and the hypothesis concerning the universality class are self-consistent or not.

To clarify the matter, let us return to the H-N transition, that is thought to be in the universality class of the classical 2D Ising model with $c = 1/2$. This can be considered as the paradigm of minimal models in CFT and the corresponding quantum field theory is that of a massless Majorana fermion. Apart from the identity (with zero scaling dimensions) one has only two primary operators with $\Delta_h = 1/16$ and $\Delta_T = 1/2$. In addition, modular invariance [46] demands that the conformal spin $(\Delta - \bar{\Delta})$ of the combinations that enter the partition function (on the torus) must be an integer (zero in this case). Hence we are left with two nontrivial primary operators of scaling dimensions $d_T = 1$ and $d_h = 1/8$, that are interpreted as energy and spin density, respectively. The former is responsible for the variations away from the critical temperature and so the correlation length index is given by $\nu = 1/(2 - d_T) = 1$. The latter, from eq. (8), gives the decay exponent of the spin-spin correlation function $\eta_z = 1/4$ at the critical point. At the same time, being $\nu = 1$ (see the following eqs. (39) and (40) in appendix B), one determines also the exponent $\beta = d_h = 1/8$, describing the opening of the magnetization away from criticality.

The GS energies at various L for the critical point ($\lambda = 1.1856, D = 0$) found above are plotted in fig. 7(b). We have seen that in the range $L = 12 - 56$ the small deviations from -1.5 are accurately fitted by the form $E_L^{GS}/L = e_\infty - cv\pi/6L^2 - A/L^{3/2} \exp(-L/\xi_1)$, with $e_\infty = -1.50093$, $cv = 1.327$, $\xi_1 = 3.48$ and $A = 1.251$. This dependence can be justified by recalling that the lattice model is mapped onto a CFT (yielding eq. (9)) for the critical sector, plus a residual Hamiltonian that accounts for the massive levels. The exponential term is what one expects in a massive regime [47], and we observe that the length ξ_1 multiplied by the finite gap with the sector $|M^z = 1|$, $\Delta E^{(1)} = 0.754$, yields $v_1 = 2.62$, a typical value of velocity (close to the one found below). In fact, at this stage we observe a non-trivial feature: the massless modes described by the CFT seem to be associated only with the levels within $M^z = 0$, while those with $M^z \neq 0$ maintain a finite energy gap in the TL. Hence, the reference state for the calculation of v will be the second excited state in $M^z = 0$, corresponding to conformal dimensions $(1/2, 1/2)$. Using eq. (10) we determine a (CFT) velocity that extrapolates to $v = 2.676 \pm 0.001$ (see fig. 8), and the resulting central charge, $c = 0.4959 \pm 0.0006$, lead us again to the 2D Ising universality class as in [29] and refs. therein. An even more stringent confirmation comes from fig. 8, that illustrates the core of the multi-target method proposed here. In table 2 we compare the theoretical values with the numerical estimates of the scaling dimensions (second column) obtained by taking the ratios between the intercepts at $1/L = 0$ of the data set in fig. 8 and the velocity pre-factor

$v = 2.676$. These intercepts, in turn, are determined using power-law fits to eliminate the residual dependence on L in a fashion similar to that of [30]. The fits are carried out in the range $L \geq 36$ because of the shoulder at $L \sim 40$ in fig. 7 that signals the onset of the scaling regime. All the multiplicities are met, even if with DMRG calculations alone we are not able to classify the four degenerate states in terms of the secondary indices. The fourth column contains the total momentum/conformal spin expected from eq. (5). Question marks indicate that the conformal continuum theory predicts 0 also for those cases that are expected to have $|Q| = \pi$ [23]. We suspect that this is due to the correspondence between the original spin model and the field theory that maps the discrete AF structure ($|Q| = \pi$) onto the low-momentum sector. Indeed, for the CFT to give $|Q| = \pi$ a secondary index equal to $L/2$ would be needed, and this would yield a nonzero energy gap in the TL. The overall agreement is good (1% in the worst cases) and the complete structure of the spectrum of the $c = 1/2$ minimal model is reproduced (only the relevant and marginal cases with $d \leq 2$ are reported). Note that all the marginal operators have nonzero momentum and so they cannot represent a valid perturbation to the continuum Hamiltonian because they would break translational invariance. The absence of marginal operators suggests that each point of the H-N transition corresponds to the same $c = 1/2$ theory and the line in the phase diagram is “generated” by the mapping of the discrete spin model onto the continuum CFT. Moving along the H-N line we expect only a change in the non-universal quantities like v , e_∞ and the values of the critical anisotropies themselves. We have seen that this is indeed the case, at least for these other two points: $[\lambda = 0.5, D_c(0.5) = -1.2]$ (left part of fig. 4) and $[\lambda = 1, D_c(1) = -0.315]$ (both found by fixing λ and varying D). For the former we get $e_\infty = -2.00120$, $v = 2.44$ and $c = 0.5008 \pm 0.0008$, while for the latter we get $v = 2.65$, $e_\infty = -1.62651$ and $c = 0.498 \pm 0.002$. The corresponding gap exponents are estimated from the decay of $\beta_L(-1.2)$ and $\beta_L(-0.315)$, with the results $\nu = 1.023 \pm 0.009$ and $\nu = 1.003 \pm 0.006$, respectively. Notice that in fig. 6 the two points have essentially the *same* β -function. After all, eqs. (35) and (37) give $\beta_L^{-1}(g_c) = C^{(1)} L^{1/\nu} \sigma_c / (2 - \nu^{-1})$, where σ_c is the derivative of $(g - g_c)$ with respect to the lattice parameter that is varied. Hence, if in fig. 6 we wish to compare the β -functions of Ising type computed at fixed λ with those computed at fixed D , we should multiply the latter by the (local) slope of H-N line $dD/d\lambda \simeq 1.697$. We have checked that with a vertical shift of $\ln 1.697 = 0.5289$ the β -function at $(\lambda = 1.185, D = 0)$ collapses onto the other two, thereby indicating that moving along the line the $c = 1/2$ conformal structure is maintained.

Concerning the discrepancy with ref. [6], we should mention that a distinctive point of their analysis is the extrapolation for $M \rightarrow \infty$. On the other hand, we feel that the numerical procedure contains two weak points. First, the conclusion that ν is not sufficiently close to 1, and the consequence that the effective dimensionality is not 2, are drawn from the estimates of the correlation length

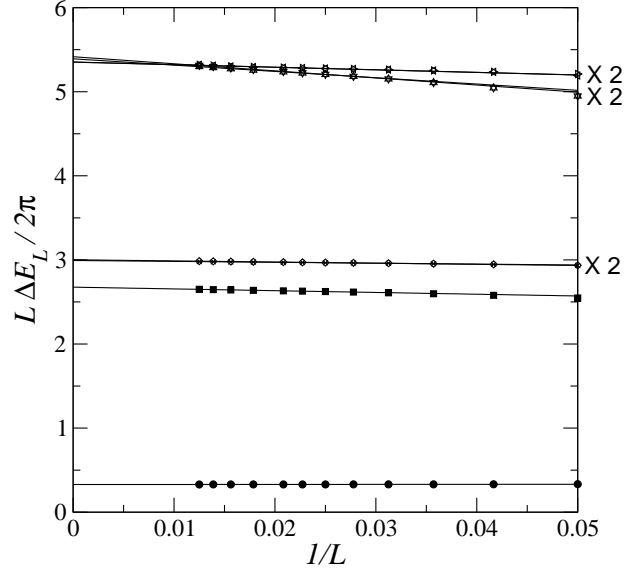


Fig. 8. Scaled gaps, divided by 2π , plotted vs $1/L$ at the Ising transition ($\lambda = 1.1856, D = 0$). Points represent the numerical values obtained with multi-target DMRG runs ($L = 20, 24, 28, 32, 36, 40, 44, 48, 56, 64, 72, 80$ with $M = 243$) collecting *eight* excited states within $M^z = 0$. Continuous lines are the best-fit whose intercepts are given in table 2, together with the theoretical predictions of the scaling dimensions (the labels on the right indicate the multiplicities).

Table 2. Spectrum of theoretical ($d_{\text{CFT}} = \Delta + \bar{\Delta} + \text{sec. indices}$) and numerical (see details in the text) conformal dimensions at the Ising transition of fig. 8.

d_{CFT} [\times multiplicity]	d_{num}	Secondary Indices	Q
0 [$\times 1$]		(0,0)	0
1/8 [$\times 1$]	0.1229 ± 0.0004	(0,0)	0 (or π ?)
1 [$\times 1$]	1	(0,0)	0 (or π ?)
9/8 [$\times 2$]	1.1185 ± 0.0008 1.1218 ± 0.0008	(1,0) (0,1)	$\pm 2\pi/L$ $\mp 2\pi/L$
2 [$\times 4$]	2.014 ± 0.005 2.025 ± 0.005 2.018 ± 0.005 2.018 ± 0.005	(2,0) (0,2) (1,0) (0,1)	$\pm 4\pi/L$ $\mp 4\pi/L$ $\pm 2\pi/L$ $\mp 2\pi/L$

using a *pure* exponential law ignoring the contribution of algebraic prefactors. According to our experience, having a multi-target code at one’s disposal, it would be better to read the values of ν directly from the excitation gap or the scaling dimension. The second and more important point is the usage of the infinite-system algorithm. In secs. 1, 3 and 4 we have given indications that this may be a risky procedure if one aims at very precise quantitative results, and that the finite-system algorithm should be preferred (see also refs. [2,19] regarding this question).

6 Concluding Remarks

The aim of this paper was to give a detailed explanation of the numerical method used to derive the results of ref. [17] and, more generally, to discuss how one can circumvent some of the problems of the DMRG close to criticality. The ideas are explicitly worked out taking some representative point in the $\lambda - D$ phase diagram for the Hamiltonian of eq. (12). In sec. 4 we have argued that close to the transition lines from the Haldane phase (at least the ones with $c = 1$) the convergence is controlled by a characteristic length $L^*(M)$ that appears to be a consequence of the truncation to the M states with the largest weights in the block density matrix ρ_b . This fact is in line with similar results by other authors [2, 4, 5], and this probably lies at the heart of the problem: in the TL the physical system behaves in a critical way but the DMRG procedure introduces a spurious length so that the numerical outcome is no longer scale invariant.

The method that we are suggesting is based on the finite-system DMRG algorithm in order to reduce as much as possible the (environment [2]) errors and has to be applied in an intermediate range of L , not too small so that the signatures of scaling are visible but not too large as compared to $L^*(M)$. Then we make use of powerful finite-size scaling predictions, coming from CFT, to extract information on the effective continuum model, like the “spin velocity” and the central charge, from the spectrum of low-lying excitations. The latter can be computed, within the DMRG, by taking ρ_b as the average of the matrices associated with a given number of excited states that, in turn, are obtained with a Thick-restart variant of the Lanczos method [15].

We think that the methods discussed here should apply also to the study of the critical behavior of other 1D quantum systems, such as Hubbard models and their generalizations [48, 49, 50, 51].

Finally, in sec. 5 we have reported some examples of $c = 1/2$ transitions between the Haldane and the Néel-like phase. In particular, we have re-examined and confirmed the 2D Ising nature of the critical point at $D = 0$ [29], which was the cause of a recent controversy [6].

7 Acknowledgements

We are grateful to L. Campos Venuti, E. Ercolessi, G. Morandi, F. Ravanini, M. Roncaglia and S.-W. Tsai for their useful interventions during the preparation of the paper. This work was partially funded by the Italian MIUR, through COFIN projects prot. n. 2002024522.001 and 2003029498.013.

Appendix A: Thick-restart Lanczos Method

Let us consider a $n \times n$ real symmetric matrix H representing the Hamiltonian operator of a quantum system in a given orthonormal basis. We are interested in the lowest eigenvalues, $\{\lambda\}$, and corresponding eigenvectors, \mathbf{x} ,

defined by the equation $H\mathbf{x} = \lambda\mathbf{x}$ (λ real, $\mathbf{x} \in \mathbb{R}^n$). If the matrix H is large and only a small number of eigenvalues are wanted, a projection-based method is generally used [52, 53]. In these methods one usually builds orthogonal bases and then performs the Rayleigh-Ritz projection to extract the approximate solutions. When the matrix is symmetric, the Lanczos method is the most commonly used algorithm, taking advantage of the fact that the actual matrix to diagonalize can be cast in tridiagonal form.

Another method used for large matrices is the Davidson one (and its variants) for which, however, the tridiagonal form is not assured. When the Hamiltonian matrix is dominated by the diagonal elements, as occurs in quantum chemistry, the Davidson-Jacobi gives very good results [53]. This does not necessarily hold for a quantum spin system in the basis of eigenstates of local S_j^z and the preconditioner (especially during the initial steps of the infinite-system algorithm) can break some of the symmetries of the Hamiltonian. Given that the choice of a particular method depends on the physical system under study, in this appendix we focus on the characteristic points of the Lanczos method used for our numerical results.

Given a starting vector $\mathbf{r}_0 \in \mathbb{R}^n$, an orthogonal sequence of vectors \mathbf{q}_i , $i = 1, 2, \dots$ is generated recursively from the relations:

$$\begin{cases} \mathbf{q}_0 = 0 \\ \beta_0 = \|\mathbf{r}_0\| \end{cases} \quad (20)$$

$$\begin{cases} \mathbf{q}_i = \frac{\mathbf{r}_{i-1}}{\beta_{i-1}} \\ \alpha_i = \langle \mathbf{q}_i, H\mathbf{q}_i \rangle \\ \mathbf{r}_i = H\mathbf{q}_i - \alpha_i\mathbf{q}_i - \beta_{i-1}\mathbf{q}_{i-1} \\ \beta_i = \|\mathbf{r}_i\|, \quad i = 1, 2, \dots \end{cases} \quad (21)$$

The vectors \mathbf{q}_i , called Lanczos vectors, form an orthonormal basis for the Krylov subspaces:

$$\mathcal{K}_m = \text{span}\{\mathbf{r}_0, H\mathbf{r}_0, \dots, H^{m-1}\mathbf{r}_0\} = \text{span}\{\mathbf{q}_1, \dots, \mathbf{q}_m\}, \quad (22)$$

and satisfy the relations:

$$H\mathbf{q}_i = \beta_{i-1}\mathbf{q}_{i-1} + \alpha_i\mathbf{q}_i + \beta_i\mathbf{q}_{i+1}, \quad (23)$$

which define a tridiagonal matrix, T_m , as a representation of H in \mathcal{K}_m :

$$T_m = \begin{pmatrix} \alpha_1 & \beta_1 & & & \\ \beta_1 & \alpha_2 & & & \\ & & \ddots & & \\ & & & \alpha_{m-1} & \beta_{m-1} \\ & & & \beta_{m-1} & \alpha_m \end{pmatrix} \quad (24)$$

The diagonalization of T_m , with $m = 1, 2, \dots$, gives eigenvalues and eigenvectors, called Ritz values and Ritz vectors, as approximate solutions to the original problem. The computation of an eigenvalue with good accuracy often requires a large number of iterations and on most machines there is not enough memory to store all the Lanczos vectors. It is necessary to limit the number m of generated vectors and restart the procedure. Since the

algorithm defined by eqs. (20) and (21) can start with one vector \mathbf{r}_0 , the usual way is to use the computed Ritz vector, if only one eigenvalue is wanted. If more than one eigenvalue is desired, we can freeze the converged ones and combine the other vectors into one starting element [53]. Other methods (Davidson-Liu or block Lanczos) are based on adding a block of states at each step but, of course, they require more computational resources. Typically, a restarting scheme needs significantly more iterations to compute a solution, but it saves memory usage. The algorithm developed by Wu and Simon [15], summarized in the following, has the advantage of adding only one vector at every step, essentially preserving the tridiagonal structure of the projected matrix.

The Thick-restart Lanczos method is based on the following observation: let us consider an arbitrary element of \mathcal{K}_m :

$$\tilde{\mathbf{q}} = \sum_{j=1}^m y_j \mathbf{q}_j, \quad y_j \in \mathbb{R} \quad (25)$$

from relation (23) we have (setting $y_0 = 0$):

$$H\tilde{\mathbf{q}} = \sum_{j=1}^m (\beta_{j-1}y_{j-1} + \alpha_j y_j + \beta_j y_{j+1}) \mathbf{q}_j + y_m \beta_m \mathbf{q}_{m+1}, \quad (26)$$

so that the residual, $\mathbf{r} = y_m \beta_m \mathbf{q}_{m+1}$, is *always parallel to \mathbf{q}_{m+1} independently from the vector $\tilde{\mathbf{q}}$ in \mathcal{K}_m and has the same direction of the residual \mathbf{r}_m computed from eq. (21) and defining \mathbf{q}_{m+1}* . This fact suggested to Wu and Simon a suitable restarting scheme.

When restarting, one has first to determine an appropriate number of Ritz vectors, say k (usually greater than the number of wanted eigenvalues):

$$\tilde{\mathbf{q}}_i = \sum_{j=1}^m q_j y_j^{(i)}, \quad i = 1, \dots, k, \quad (27)$$

corresponding to the Ritz values λ_i . The chosen Ritz vectors contain the best approximations available for the wanted eigenvectors. Since the matrix T_m is symmetric, there is no reason to use any basis set different from its eigenvectors:

$$T_m \mathbf{y}^{(i)} = \lambda_i \mathbf{y}^{(i)}, \quad i = 1, \dots, k \quad (28)$$

(We denote with a tilde the quantities after the restart, to distinguish them from the corresponding ones before the restart.) Using these k vectors, the projected matrix of H , \tilde{T}_k , is diagonal and the vectors satisfy the relations:

$$H\tilde{\mathbf{q}}_i = \lambda_i \tilde{\mathbf{q}}_i + y_m^{(i)} \beta_m \tilde{\mathbf{q}}_{k+1}, \quad i = 1, \dots, k, \quad (29)$$

with $\tilde{\mathbf{q}}_{k+1} = \mathbf{q}_{m+1}$. So we can enlarge the basis $\{\tilde{\mathbf{q}}_1, \dots, \tilde{\mathbf{q}}_k\}$ with the vector $\tilde{\mathbf{q}}_{k+1}$ and, using the symmetry of the matrix H , the vector $\tilde{\mathbf{q}}_{k+2}$ can be computed by the residual:

$$\mathbf{r}_{k+1} = H\tilde{\mathbf{q}}_{k+1} - \tilde{\alpha}_{k+1} \tilde{\mathbf{q}}_{k+1} - \sum_{j=1}^k \beta_m y_m^{(j)} \tilde{\mathbf{q}}_j. \quad (30)$$

Correspondingly, the matrix \tilde{T}_k is extended by one row and one column into the matrix \tilde{T}_{k+1} . The latter is not

tridiagonal as the original T_m but further steps follow the three-terms relations (23), defining $\tilde{\alpha}_i$ and $\tilde{\beta}_i$ for $i = k+2, k+3, \dots, m$, and at step $m > k+1$ we have the following form for \tilde{T}_m :

$$\tilde{T}_m = \begin{pmatrix} \lambda_1 & & & \tilde{\beta}_1 & & \\ & \ddots & & \vdots & & \\ & & \lambda_k & \tilde{\beta}_k & & \\ \tilde{\beta}_1 & \dots & \tilde{\beta}_k & \tilde{\alpha}_{k+1} & \tilde{\beta}_{k+1} & \\ & & & \tilde{\beta}_{k+1} & \tilde{\alpha}_{k+2} & \\ & & & & & \ddots \end{pmatrix} \quad (31)$$

with $\tilde{\beta}_i = \beta_m y_m^{(i)}$, $i = 1, \dots, k$. Since the vectors in the new subspace generated by $\{\tilde{\mathbf{q}}_1, \dots, \tilde{\mathbf{q}}_m\}$ have the same property that the residual is always parallel to $\tilde{\mathbf{q}}_{m+1}$, the procedure can be repeatedly restarted, until we find a good convergence of the wanted eigenvalues. The matrix T_m is no longer tridiagonal after the first restart, but it can still be stored and diagonalized in an efficient way. It is easy to arrange the algorithm so that \mathbf{q}_i and $\tilde{\mathbf{q}}_i$ occupy the same memory locations.

We can summarize saying that the restarting scheme with k Ritz vectors \mathbf{q}_i (we now drop the tilded notation), and a residual \mathbf{r}_k satisfying the rule:

$$H\mathbf{q}_i = \lambda_i \mathbf{q}_i + \beta_i \mathbf{q}_{k+1}, \quad (32)$$

with $\mathbf{q}_{k+1} = \mathbf{r}_k / \|\mathbf{r}_k\|$, is composed by an initialization:

$$\begin{cases} \alpha_{k+1} = \langle \mathbf{q}_{k+1}, H\mathbf{q}_{k+1} \rangle \\ \mathbf{r}_{k+1} = H\mathbf{q}_{k+1} - \alpha_{k+1} \mathbf{q}_{k+1} - \sum_{j=1}^k \beta_j \mathbf{q}_j \\ \beta_{k+1} = \|\mathbf{r}_{k+1}\| \end{cases} \quad (33)$$

followed by typical Lanczos iterations (eq. (21)) for $i = k+2, k+3, \dots, m$.

This concludes our description of the Thick-restart Lanczos algorithm. We refer to the original paper [15] for a detailed discussion of the errors and precision of the method.

Appendix B: Brief Survey of FSS Theory

Ideally, we should locate the critical points of a quantum system by looking at the smallest energy gap, ΔE , as a function of a (relevant) parameter g and identify g_c through the condition $\Delta E(g_c) = 0$. For an algebraic transition the critical index ν controls the opening of the gap, $\Delta E \propto |g - g_c|^\nu$. However, when the critical point is approached numerically we encounter two related problems. First, the system's size is necessarily finite and a true phase transition is forbidden. Second, if we are able to deal with sufficiently large systems close to g_c , the energy gap may become so small as to be comparable with the errors introduced by the algorithm (or, ultimately, by the machine). Hence we need a prescription to infer the location of the critical point from nonzero values of ΔE_L at finite L .

In FSS theory [24,45,54] one usually invokes the following ansatz (quantum Hamiltonian notations):

$$\Delta E_L = \frac{1}{L} F(\zeta), \quad \zeta \equiv L^{1/\nu} |g - g_c|, \quad (34)$$

so that the scaling variable ζ covers these two regimes

- (a) $\zeta \rightarrow 0$ for $g \rightarrow g_c$ at fixed L . In this regime we should see a finite system at the infinite-size critical point. Since ΔE_L is in fact an inverse correlation length ξ_L , we expect the latter to be as large as possible, that is to say $\Delta E_L \propto L^{-1}$. Compatibility with eq. (34) then requires $F(0) \neq 0$. This is exactly the case for which the continuum description of CFT applies (sec. 2). Hence, recalling that the scaling dimension of the gap-generating operator is $(2 - \nu^{-1})$, we may write $F(0) = 2\pi\nu(2 - \nu^{-1})$ and expand $F(\zeta)$ in a McLaurin series for $\zeta \ll 1$:

$$\Delta E_L = \frac{2\pi\nu}{L} [(2 - \nu^{-1}) + C^{(1)}\zeta + C^{(2)}\zeta^2 + \dots]. \quad (35)$$

- (b) $\zeta \rightarrow \infty$, which means $(L/\xi_L)^{1/\nu} \gg 1$. This regime mimics the TL, in the sense that ξ_L is large but finite because the system is slightly off-critical and L is sufficiently large so that scaling laws appear. Hence L must effectively cancel in eq. (34), leaving just $|g - g_c|^\nu$. This is possible if:

$$F(\zeta) \sim \zeta^\nu \quad \zeta \gg 1. \quad (36)$$

From (a) we derive the way to locate the critical points through FSS: Plot $\ln(\Delta E_L)$ vs $\ln L$ and look for the value of g that best gives a straight line with slope -1 . Actually, we can be even more severe by looking for slope 0 in the curves of the scaled gaps $L\Delta E_L$. As far as the index ν is concerned, one may consider the finite-size β -function, $\beta_L^{-1}(g) \equiv \partial \ln(\Delta E_L) / \partial g$, evaluated at $g = g_c$ as determined above (apart from the sign):

$$\beta_L(g_c) = [F(\zeta)/F'(\zeta)]_{\zeta=0} L^{-1/\nu}, \quad (37)$$

where F' denotes the derivative with respect to ζ and $F'(0)$ is also assumed to be nonzero. In principle $\beta_L(g_c)$ should vanish with an exponent $1/\nu$ that represents the asymptotic slope in log-log scales. Alternatively, since the scaling region may be reachable only for very large L , one can calculate the discrete logarithmic derivative through a size increment $L \rightarrow L + \delta L$:

$$\frac{1}{\nu_L} \equiv - \frac{\ln \beta_{L+\delta L}(g_c) - \ln \beta_L(g_c)}{\ln(L + \delta L) - \ln L}, \quad (38)$$

and this should converge to $1/\nu$ when $L \rightarrow \infty$.

Finally, the ansatz (34) can be generalized to other physical quantities that behave as $\mathcal{Q}(g) \propto |g - g_c|^{\nu_Q}$ near the critical point:

$$\mathcal{Q}_L(g) = L^{-z_Q} F_Q(\zeta), \quad (39)$$

with the same scaling variable ζ and scaling exponent z_Q . As above, in the critical regime (a) $\zeta \rightarrow 0$ we shall require

$F_Q(0) \neq 0$, while in the off-critical regime (b) the scaling exponent ν_Q emerges provided that $F_Q \sim \zeta^{\nu_Q}$ for $\zeta \rightarrow \infty$, and $z_Q = \nu_Q/\nu$. In many cases, \mathcal{Q}^2 is a squared order parameter given by the asymptotic value of a certain correlation function, $\langle O_Q(0)O_Q(r) \rangle$, that slightly away from the critical point behaves as:

$$\langle O_Q(0)O_Q(r) \rangle \propto \frac{G_Q(r/\xi)}{r^{2d_Q}}, \quad (40)$$

d_Q being the scaling dimension of O_Q . At this stage we can make the scaling argument of Ginsparg (sec. 5.1 of [16]) evaluating eq. (40) just at the correlation length itself, $r = \xi \propto |g - g_c|^{-\nu}$ thereby having $\langle O_Q(0)O_Q(\xi) \rangle \sim \mathcal{Q}^2 \sim G_Q(1)|g - g_c|^{2\nu d_Q}$. Hence we find the scaling law $d_Q = \nu_Q/\nu$, that tells us that z_Q in eq. (39) is nothing but the scaling dimension of the operator associated with the order parameter \mathcal{Q} . In ref. [17] we have used this property to derive the decay exponents of ordinary (transverse channel) and string (z -channel) correlation functions in $c = 1$ phases by applying eq. (39) to the corresponding Néel and string order parameters evaluated at half chain.

References

1. For an introduction and a series of applications of the DMRG see: I. Peschel, X. Wang, M. Kaulke and K. Hallberg (editors), *Density-Matrix Renormalization - A New Numerical Method in Physics* (Berlin, Springer, 1999).
2. Ö. Legeza and G. Fáth, Phys. Rev. B **53**, 14349 (1996).
3. Ö. Legeza, J. Röder and B. A. Hess, Phys. Rev. B **67**, 125114 (2003).
4. M. Andersson, M. Boman and S. Östlund, Phys. Rev. B **59**, 10493 (1999).
5. T. Nishino, K. Okunishi and M. Kikuchi, Phys. Lett. A **213**, 69 (1996).
6. M. Capone, S. Caprara and L. Cataldi, *Quantum phase transition in easy-axis anti-ferromagnetic integer-spin chains*, e-print at <http://arxiv.org/abs/cond-mat/0307266>.
7. J. B. Kogut, Rev. Mod. Phys. **51**, 659 (1979).
8. A. B. Zamolodchikov and V. Fateev, Sov. J. Nucl. Phys. **32**, 298 (1980).
9. I. Peschel, M. Kaulke and Ö. Legeza, Ann. Phys. (Leipzig) **8**, 153 (1999).
10. K. Okunishi, Y. Hieida and Y. Akutsu, Phys. Rev. E **59**, R6227 (1999).
11. P. Di Francesco, P. Mathieu and D. Senechal, *Conformal Field Theory* (New York etc., Springer, 1997).
12. F. Ravanini, *Finite Size Effects in Integrable Quantum Field Theory*, Lectures given at the Eötvös Summer School, Budapest, August 2000, e-print at <http://arxiv.org/abs/hep-th/0102148>.
13. S. R. White, Phys. Rev. B **48**, 10345 (1993).
14. R. J. Bursill, Phys. Rev. B **63**, 157101 (2001).
15. K. Wu and H. Simon, SIAM J. Matrix Anal. Appl. **22**, 602 (2000).
16. P. Ginsparg in *Fields, Strings and Critical Phenomena: Les Houches 1988, Session XLIX*, edited by E. Brézin and J. Zinn-Justin (Amsterdam etc., North-Holland, 1990).

17. C. Degli Esposti Boschi, E. Ercolessi, F. Ortolani and M. Roncaglia, *Eur. Phys. J. B* **35**, 465 (2003).
18. H. W. J. Blöte, J. L. Cardy and M. P. Nightingale, *Phys. Rev. Lett.* **56**, 742 (1986).
19. S.-W. Tsai and J. B. Marston, *Phys. Rev. B* **62**, 5546 (2000).
20. R. J. Bursill, R. H. McKenzie and C. J. Hamer, *Phys. Rev. Lett.* **80**, 5607 (1998).
21. I. Affleck, *Phys. Rev. Lett.* **56**, 746 (1986).
22. A. Kitazawa, *J. Phys. A: Math. Gen.* **30**, L285 (1997).
23. R. Botet, R. Jullien and M. Kolb, *Phys. Rev. B* **28**, 3914 (1983).
24. U. Glaus and T. Schneider, *Phys. Rev. B* **30**, 215 (1984).
25. H. J. Schulz, *Phys. Rev. B* **34**, 6372 (1986).
26. T. Kennedy and H. Tasaki, *Commun. Math. Phys.* **147**, 431 (1992).
27. W. Chen, K. Hida and B. C. Sanctuary, *Phys. Rev. B* **67**, 104401 (2003).
28. S. R. White, *Phys. Rev. Lett.* **69**, 2863 (1992).
29. A. Kitazawa and K. Nomura, *J. Phys. Soc. Japan* **66**, 3944 (1997).
30. W. Chen, K. Hida and B. C. Sanctuary, *J. Phys. Soc. Japan* **69**, 237 (2000).
31. S. R. White and R. L. Martin, *J. Chem. Phys.* **110**, 4127 (1999).
32. M. C. Chung and I. Peschel, *Phys. Rev. B* **64**, 064412 (2001).
33. F. D. M. Haldane, *Phys. Rev. Lett.* **50**, 1153 (1983).
34. M. den Nijs and K. Rommelse, *Phys. Rev. B* **40**, 4709 (1989).
35. G. Xu, J. F. DiTusa, T. Ito, K. Oka, H. Takagi, C. Broholm and G. Aeppli, *Phys. Rev.* **54**, R6827 (1996).
36. J. Darriet and L. P. Regnault, *Solid State Comm.* **86**, 409 (1993).
37. J. Sólyom and T. A. L. Ziman, *Phys. Rev. B* **30**, 3980 (1984).
38. L. P. Regnault, I. Zaliznyak, J. P. Renard and C. Vettier, *Phys. Rev. B* **50**, 9174 (1994).
39. I. A. Zaliznyak, D. C. Dender, C. Broholm and D. H. Reich, *Phys. Rev. B* **57**, 5200 (1998).
40. M. Orendác, S. Zvyagin, A. Orendáčová, M. Sieling, B. Lüthi, A. Feher and M. W. Meisel, *Phys. Rev. B* **60**, 4170 (1999).
41. R. Jullien and P. Pfeuty, *J. Phys. A: Math. Gen.* **14**, 3111 (1981).
42. F. C. Alcaraz and Y. Hatsugai, *Phys. Rev. B* **46**, 13914 (1992).
43. A. Anfossi and A. Montorsi, private communication.
44. M. E. Gouvêa and A. S. T. Pires, *Phys. Rev. B* **63**, 134408 (2001).
45. C. J. Hamer and M. N. Barber, *J. Phys. A: Math. Gen.* **14**, 241 (1981).
46. J. L. Cardy in *Fields, Strings and Critical Phenomena: Les Houches 1988, Session XLIX*, edited by E. Brézin and J. Zinn-Justin (Amsterdam etc., North-Holland, 1990).
47. S. Qin, Y.-L. Liu and L. Yu, *Phys. Rev. B* **55**, 2721 (1997).
48. S. Daul and R. M. Noack, *Phys. Rev. B* **58**, 2635 (1998).
49. G. Fano, F. Ortolani, A. Parola and L. Ziosi, *Phys. Rev. B* **60**, 15654 (1999).
50. G. P. Zhang, *Phys. Rev. B* **68**, 153101 (2003); E. Jeckelmann, *Phys. Rev. Lett.* **89**, 236401 (2002).
51. J. Lou, S. Qin, T. Xiang, C. Chen, G.-S. Tian and Z. Su, *Phys. Rev. B* **68**, 045110 (2003).
52. B. N. Parlett, *The Symmetric Eigenvalue Problem*, *Classics Appl. Math.* 20 (Philadelphia, SIAM, 1998).
53. Y. Saad, *Numerical Methods for Large Eigenvalue Problems* (Manchester, Manchester University Press, 1993).
54. M. E. Fisher and M. N. Barber, *Phys. Rev. Lett.* **28**, 1516 (1972).